Journal of Chromatography A, 1422 (2015) 299–309

Contents lists available at ScienceDirect

Journal of Chromatography A

journal homepage: www.elsevier.com/locate/chroma

Toward a microfabricated preconcentrator-focuser for a wearable micro-scale gas chromatograph

Jonathan Bryant-Genevier[a,c], Edward T. Zellers[a,b,c,*]

[a] Department of Environmental Health Sciences, University of Michigan, Ann Arbor, MI 48109-2029, United States
[b] Department of Chemistry, University of Michigan, Ann Arbor, MI 48109-2029, United States
[c] Center for Wireless Integrated MicroSensing & Systems, University of Michigan, Ann Arbor, MI, United States

ARTICLE INFO

Article history:
Received 17 July 2015
Received in revised form 14 October 2015
Accepted 14 October 2015
Available online 17 October 2015

Keywords:
Preconcentrator
Microfabricated
Micro gas chromatography
Benzene
VOC mixture

ABSTRACT

This article describes work leading to a microfabricated preconcentrator-focuser (μPCF) designed for integration into a wearable microfabricated gas chromatograph (μGC) for monitoring workplace exposures to volatile organic compounds (VOCs) ranging in vapor pressure from ~0.03 to 13 kPa at concentrations near their respective Threshold Limit Values. Testing was performed on both single- and dual-cavity, etched-Si μPCF devices with Pyrex caps and integrated resistive heaters, packed with the graphitized carbons Carbopack X (C-X) and/or Carbopack B (C-B). Performance was assessed by measuring the 10% breakthrough volumes and injection bandwidths of a series of VOCs, individually and in mixtures, as a function of the VOC air concentrations, mixture complexity, sampling and desorption flow rates, adsorbent masses, temperature, and the injection split ratio. A dual-cavity device containing 1.4 mg of C-X and 2.0 mg of C-B was capable of selectively and quantitatively capturing a mixture of 14 VOCs at low-ppm concentrations in a few minutes from sample volumes sufficiently large to permit detection at relevant concentrations for workplace applications with the μGC detector that we ultimately plan to use. Thermal desorption at 225 °C for 40 s yielded ≥99% desorption of all analytes, and injected bandwidths as narrow as 0.6 s facilitated efficient separation on a downstream 6-m GC column in <3 min. A preconcentration factor of 620 was achieved for benzene from a sample of just 31 mL. Increasing the mass of C-X to 2.3 mg would be required for exhaustive capture of the more volatile target VOCs at high-ppm concentrations.
© 2015 Elsevier B.V. All rights reserved.

1. Introduction

Measuring personal exposures to mixtures of airborne volatile organic compounds (VOCs) in working environments by standard methods entails the collection of breathing-zone air samples with adsorbent-packed devices followed by analysis at an off-site laboratory [1–4]. Since sample durations are typically several hours, only average (e.g., daily) concentrations are obtained; exposure dynamics within a work shift are lost. Gathering near-real-time measurements could improve the quality of exposure data [5]. Yet, current portable direct-reading VOC-monitoring instruments capable of quantitative multi-VOC determinations, which employ gas chromatographic (GC) separations and/or spectrometric detectors, remain too large, complex, and expensive for routine deployment as personal exposure monitors [6–9].

In attempts to address some of the shortcomings of conventional portable GC instrumentation, significant efforts by several research groups over the past four decades have been devoted to developing GC microsystems (μGC) constructed from Si-microfabricated components, with steady progress being made toward smaller packages with lower power dissipation and greater analytical capabilities [10–22]. Most μGC systems contain a micropreconcentrator or other on-board injection device, one or more separation microcolumns, and a microsensor or microsensor array detector, along with the necessary auxiliary hardware and software for standalone or computer-controlled operation. The micropreconcentrator provides the means to trap VOCs from an air sample, typically by adsorption on a granular solid, and then to thermally desorb and inject them as a focused band for subsequent separation and detection. The dual functions demanded of this μGC component are reflected in the term "micropreconcentrator-focuser" (μPCF) [23–25], and the range of μPCF designs, adsorbent materials, and operating features reported over the past decade reflect the challenges to optimizing performance while minimizing size and power dissipation (for examples, see Refs. [23–38]).

* Corresponding author at: Department of Environmental Health Sciences, University of Michigan, Ann Arbor, MI 48109-2029, United States.
E-mail address: ezellers@umich.edu (E.T. Zellers).

http://dx.doi.org/10.1016/j.chroma.2015.10.045
0021-9673/© 2015 Elsevier B.V. All rights reserved.

In most reported μPCF devices, only a fraction of the mass of any targeted VOC(s) in the air passing through the device is captured and subsequently desorbed for analysis [28,30,31,33,34,37]. As with classical solid-phase microextraction (SPME) [39,40], these devices rely on the equilibrium that can be established between the VOC air concentration and the VOC surface concentration to relate the former to the latter upon subsequent quantification. Complementing such *equilibrium* μPCFs is another class of devices that capture the entire mass of any targeted VOC(s) in the air sample [23–25,27,32,35,36]. Despite their generally larger size and consequently greater heating power dissipation, these so-called *exhaustive* μPCFs yield much larger preconcentration factors (PF) [23,24,41,42], and the relationship between VOC air concentrations and analyzed quantities of VOCs is more direct. In fact, although significant sensitivity enhancements can be achieved with *equilibrium* μPCF devices [31,33], since an unknown fraction of the total sampled VOC mass is lost, bonafide PF values cannot be calculated [41,42].

The design and operation of exhaustive μPCF devices are subject to several constraints. A certain minimum sample volume is required to ensure that the mass of analyte(s) collected exceeds the limit(s) of detection (LOD) of the downstream microsensor(s), while the maximum sample volume is constrained by the inherently low capacities of the small quantities of adsorbent materials used. Flow rate, bed residence time, temperature, ambient water vapor and background VOC concentrations, adsorbent mass and specific surface area, and analyte volatility and functionality are all factors affecting capacity. Many of these same factors also affect the efficiency of thermal desorption and the minimum injection band width achievable. Thus, several aspects of μGC system performance are contingent upon the performance of the μPCF component.

Using the modified Wheeler Model as a guide, Lu and Zellers established relationships between the breakthrough volume (V_b), adsorbent bed mass, bed residence time (τ), and challenge concentration in their studies of small single- and multi-adsorbent packed-capillary PCF devices intended for use in portable GC instruments [23,24]. Systematic tests of capacity and desorption bandwidth for individual VOCs and VOC mixtures were performed with a selected set of adsorbents to establish the minimum required adsorbent masses and maximum allowable flow rates for exhaustive trapping and efficient desorption. These studies provided the basis for the adsorbent masses used in the first-generation μPCF devices of the early μGC systems developed in our group [13,25,26].

Later work by Sukaew et al. [36], examined in greater detail the relationships between values of V_b and τ of individual VOCs for a series of capillary-style PCFs and next-generation μPCFs packed with the graphitized carbon Carbopack X (C-X). They showed that below a minimum "safe" bed residence time, τ_{safe}, the bed efficiency was <60% and the dependence of V_b on flow rate was extremely sharp and, therefore, unstable to minor fluctuations in flow rate. They recommended as a generic guideline operating at flow rates that would maintain $\tau > \tau_{safe}$. Indeed, the operating conditions of μPCF devices incorporated into two subsequently developed application-specific μGC systems were guided by such considerations [16,20,21,32].

In this article we describe the development and characterization of a μPCF for use, ultimately, in a wearable μGC system referred to as a personal exposure monitoring microsystem (PEMM), currently under development in our laboratory. The instrument is intended for generalized VOC measurements in industrial workplace environments, and we set out goals of quantitatively analyzing ~10–20 VOCs per measurement at a rate of 6–8 measurements per hour, where the VOCs would all fall within a specified volatility window defined by their vapor pressures; concentrations might range over several orders of magnitude, but for quantification most or all would be at parts-per-billion (ppb) to parts-per-million (ppm) levels. Reconciling the constraints these place on the μPCF with those related to the separation efficiency of the microcolumns and the sensitivities of the microsensor array to be employed required careful assessment of the tradeoffs to achieve satisfactory system-level performance. Using a set of extant μPCF devices, we determined the adsorbent masses and operating conditions that would be required for a new dual-adsorbent μPCF to achieve selective, exhaustive preconcentration and efficient, sharp injection of mixtures of VOCs with vapor pressures, p_v, in a designated range, at concentrations relevant to demonstrating compliance with current occupational exposure limits.

As further background for our study, in the next section we introduce the PEMM microsystem and describe the detailed competing performance criteria affecting the design of the new μPCF. The resulting performance specifications for this application are then presented along with their rationales and associated compromises. The test set of VOCs is presented and ranges of concentrations, flow rates, and sampling times are defined on the basis of such considerations. We then proceed to describe our methodology and the results of testing with representative quantities of the adsorbent materials to be used to determine conditions for optimal desorptions/injections. The effects of key variables on the dynamic adsorption capacity are then presented followed by a final performance demonstration with a moderately complex mixture of target and interfering VOCs. Note that all testing reported here used conventional bench-scale GC instrumentation for separation and detection.

2. Experimental design and rationale

Fig. 1 shows a block diagram of one of the analytical subsystem layouts being considered for the first PEMM μGC prototype currently being developed. The primary analytical/fluidic components

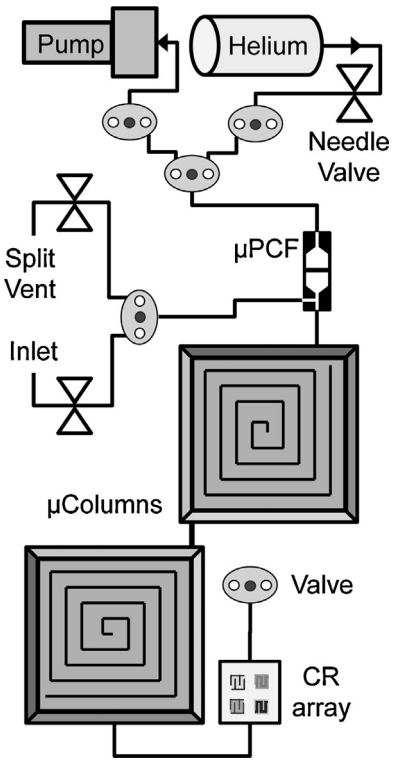

Fig. 1. Fluidic layout of the proposed PEMM μGC. VOCs from air samples drawn through the inlet by the on-board mini-pump would be captured in the μPCF and then thermally desorbed and backflushed into the first separation μcolumn on a background of He gas.

are being fabricated on discrete Si chips and consist of a dual-cavity (dual-adsorbent) μPCF, two series-coupled separation microcolumns (each 3-m long; ~3 cm × 3 cm footprint), and an integrated array of chemiresistor (CR) microsensors that employs a set of complementary thiolate-monolayer-protected gold nanoparticles (MPN) as partially selective, sorptive interface layers. Commercial mini-valves and mini-pumps are to be used along with a carrier gas of helium from an on-board canister. A pre-trap will be added at the inlet to remove low-volatility interferences. This analytical subsystem shares several basic features with those of an earlier prototype developed in our group [16,32]. Among the refinements to be incorporated into the PEMM prototype are the elimination of the high-volume sampler module required previously to achieve sub-ppb LODs, use of a dual-cavity μPCF, a split-injection valve, an on-board carrier gas source, a stream-lined fluidic system, and a smaller and more robust physical layout.

In operation, the on-board mini-pump would draw an air sample of a pre-set volume through the pre-trap and μPCF so that VOCs in the specified p_v range are captured on the μPCF. Then, the appropriate valves would be thrown, passing carrier gas through the μPCF as it is rapidly, resistively heated to backflush the desorbed VOCs in a focused injection plug to the head of the first microcolumn. This would be followed by temperature-programmed separation, and subsequent detection, identification and quantification of the target VOCs by the CR array.

Defining the nature, number, and concentration ranges of target VOCs was necessary at the outset in order to specify the types and, ultimately, amounts of adsorbent materials to use in the μPCF. One criterion used to delimit the target VOCs was that they had to fall within a p_v range of ~0.03–13 kPa (i.e., 0.2 to ~95 mm Hg). Less volatile compounds would tend to accumulate on surfaces and components in the fluidic pathways, and more volatile compounds would be more difficult to trap, separate, and detect. Selective preconcentration is, in fact, an essential element of all μGC system designs because of the relatively short microcolumns used and limited peak capacities available.

Another criterion used to define the targets was that they had Threshold Limit Values (TLV®) issued by the American Conference of Governmental Industrial Hygienists [43], which are generally in the high-ppb to mid-ppm range. Thus, we had benchmarks for the range of concentrations on which to focus for this application (e.g., 0.1–2 × TLV). The selection of interferences was not so constrained, and for testing purposes we chose to include just a few representative compounds with p_v values higher than the range specified above, in order to demonstrate the degree of selectivity achievable with the μPCF. Less volatile interferences were not included here because we have not yet finalized the design of the pre-trap we intend to include in the PEMM for precluding their capture. As to the number of targets to include, the decision was somewhat arbitrary because the PEMM μGC is intended for a wide variety of targets, the nature and number of which would change with the application. We settled on 14 target VOCs with the expectation that, for many applications, fewer would need to be analyzed, but other VOCs within the specified volatility range could be present; that is, VOCs that are targets in one situation could be a potential interferences in another. Table 1 lists the set of target VOCs used in this study, along with their p_v values and TLV values.

Establishing limits of detection (LOD) was then necessary in order to specify the minimum air sample volume and the associated volumetric flow rate of the sampling step. Since practitioners often consider 0.1 × TLV as a useful level to consider the hazard from a given chemical to be acceptably low [2], we adopted this as a benchmark value. For benzene, which has the lowest TLV among our targets (Table 1), this corresponds to 0.05 ppm, and for ethyl acetate, with the highest TLV of 400 ppm, it corresponds to 40 ppm. Previous testing performed with the type of CR array to be used as the PEMM detector indicated that a minimum sample mass of ~5 ng would ensure detection by at least two microsensors in an array for VOCs in the specified volatility range [44,45]. Assuming exhaustive trapping by our μPCF, then the sample volumes required to achieve the desired LODs would span from 0.040 mL for ethyl acetate to 32 mL for benzene. If we then set a maximum concentration limit of 2 × TLV, which would represent an excessively high concentration, this would correspond to 1.0 ppm for benzene and 800 ppm for ethyl acetate. If we further place the constraint that these concentrations should create responses that are 20 × LOD, then the required sample volumes would be the same as those quoted above for 0.1 × TLV levels.

Table 1
17 test compounds with corresponding vapor pressures (p_v) and TLVs.

Compound	Peak #[a]	p_v [b] (kPa)	TLV[c] (ppm)
Dichloromethane (DCM)[d]	2	58.0	50
Acetone (ACE)[d]	1	31.5	500
2-Butanone (MEK)[d]	3	13.3	200
Benzene (BEN)	6	12.6	0.5
1,2-Dichloroethane (DCA)	5	10.5	10
Ethyl acetate (EAC)	4	9.71	400
Trichloroethylene (TCE)	7	6.25	10
Toluene	9	3.78	20
Methyl isobutyl ketone	8	2.65	20
n-Butyl acetate	11	1.53	150
2-Hexanone	10	1.46	5
Ethylbenzene	12	1.27	20
m-Xylene	13	1.01	100
Cumene	14	0.60	50
1,2,4-Trimethylbenzene	15	0.27	25
Nitrobenzene	16	0.033	1
n-Dodecane	17	0.027	–[e]

[a] Peak assignments for chromatogram in Fig. 6b.
[b] Values at 25 °C.
[c] TLV-TWA; Ref. [43].
[d] High-volatility interferences.
[e] No assigned TLV value.

Note, however, that the range of TLV values assigned to our set of target compounds is 800-fold, and by stipulating a dynamic range of 0.1–2 × TLV for each target, the range of desired measurable concentrations spanned by the target list is from 0.05 (benzene) to 800 ppm (ethyl acetate), or 16,000-fold! The corresponding range of masses this represents was deemed infeasible to analyze, much less trap exhaustively on a μPCF in a single sample, and it illustrates an important challenge for this application. In response to this, we are considering two operating modes for the instrument; one when relatively low VOC concentrations would be anticipated, and another when higher concentrations would be anticipated. Pending a more definitive delineation of "low" and "high" concentrations, for the latter, we have set a provisional minimum sample volume of 10 mL, such that, even in the presence of co-contaminants at high concentrations, benzene could still be measured at its TLV with a signal corresponding to 3 × LOD. At the same time, the captured masses of other VOCs would not be excessive.

Given the ranges of structures and vapor pressures among our target VOCs, and taking into account previous experience in our group on this topic [23–26,32–34,36], we selected the graphitized carbons C-X and Carbopack B (C-B) as suitable adsorbent materials to use in the dual-cavity μPCF. The former has been shown to have the right combination of adsorption capacity and desorption efficiency for VOCs with p_v values from ~4.0 to 13 kPa, while the latter shows similar suitability for VOCs with p_v values from ~0.01 to 4 kPa. Both are hydrophobic.

To specify a *minimum* flow rate required placing a limit on the time allotted for this step in the duty cycle of the instrument. Since we wished to collect measurements over a relatively short time period to capture short-term variations in exposure,

but we were not concerned with acute health effects arising from extremely high exposures, we settled on a 10-min cycle time as a provisional specification, i.e., 1 sample every 10 min. Anticipating ~4 min for injection/separation/detection, and ~1 min for re-setting parameters after each analysis, ~5 min could be allotted to sample collection. For sample volumes of 10–35 mL, the range of minimum flow rates would then be ~2–7 mL/min.

The *maximum* flow rate would then be dictated primarily by two factors: the LODs and the values of τ_{safe}. Having set 5 ng as a reasonable minimum sample mass, as shown above, it would require sample volumes between 0.040 and 32 mL to capture such a quantity for measurements at 0.1 × TLV for all target VOCs. From previous work with a C-X packed single-cavity μPCF device [36], a τ value of 20 ms would yield 90% bed efficiency for our most volatile target, benzene (i.e., $\tau \gg \tau_{safe}$). For the cavity sizes of the devices available for this study this would correspond to flow rates between 8.5 and 14 mL/min. At these flow rates it would require only a few seconds to capture sufficient mass for reliable analysis of several target VOCs at the concentrations under consideration. Other factors, such as internal flow-path dead volumes that demand somewhat larger sample volumes, place additional constraints on the maximum flow rate. Assuming a similar value of τ is needed to achieve similar bed efficiencies for the most volatile VOCs to be captured in the device cavity packed with C-B, then similar constraints on maximum flow rates would apply, and the smaller of the two beds would govern the maximum flow rate.

Of course, the influence of co-contaminants on the breakthrough volumes of target VOCs must also be included in any comprehensive study. Toward this end, the compound expected to have the lowest value of V_b on each adsorbent bed would be designated as the "sentinel" for the other compounds, and limits on sample volumes could be set accordingly [23,24].

To ensure negligible carryover of samples from run to run, the desorption efficiency (DE) must be as close to 100% as possible. Desorption bandwidth is also important, as the downstream chromatographic resolution is affected by the sharpness of the injection band. For assessing DE, a focus would naturally be placed on compounds with low p_v values, which are the most difficult to volatilize from the adsorbent surface. For assessing bandwidth, compounds with high p_v values and short retention times would be of greater concern, since they are more difficult to resolve chromatographically.

3. Experimental methods

3.1. Materials

All test compounds were purchased from Sigma–Aldrich/Fluka (Milwaulkee, WI) or Acros/Fisher (Pittsburgh, PA) in >95% (most >99%) purity and were used as received. Samples of C-B and C-X (60/80 mesh, Supelco, Bellefonte, PA) were sieved to isolate fractions with nominal diameters of 212–250 μm.

3.2. Devices

The dual-cavity μPCF devices used here are designated as μPCF-2 and the single cavity devices are designated as μPCF-1x or μPCF-1b depending on whether they were loaded with C-X or C-B, respectively. As with the μPCF-1 devices, described previously [28,32], the 4.2 mm × 12.1 mm μPCF-2 chips were fabricated from 500-μm thick Si wafers using deep-reactive-ion-etching to create all features. The central cavity, inlet/outlet ports, and the tee-junction adjacent to one side of the cavity were all 380-μm deep (see Fig. 2). Cylindrical pillars (150-μm spacing and widths) were added just inside the cavity inlet and outlet to retain adsorbent granules, and to divide the cavity into front and back sub-sections, with volumes of 4.7 μL and 2.9 μL, respectively. The walls of the cavity tapered toward the inlet and outlet to reduce turbulence and promote even distribution of the flow stream. Filling ports etched into the sidewalls of each subsection were used for loading adsorbent granules. A 120-μm thick Pyrex plate was anodically bonded to the top surface at wafer level to seal the tops of the devices. Two Ti/Pt contact pads along with a resistive temperature device (RTD) were evaporated onto the backside of the Si for bulk resistive heating and temperature monitoring, respectively. Devices were then diced into individual chips.

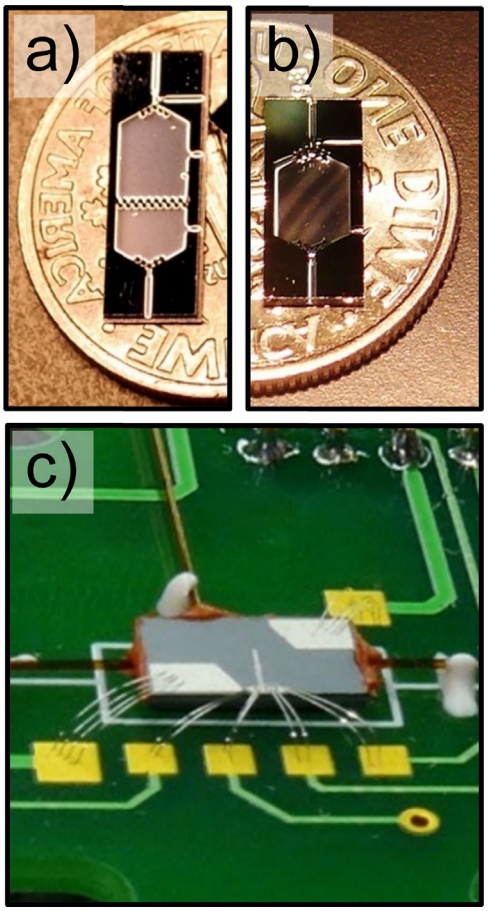

Fig. 2. Photographs of (a) μPCF-2; and (b) μPCF-1 devices (on U.S. dimes for scale); (c) μPCF-2 inverted and mounted to a custom printed circuit board; device is suspended by the inlet/outlet capillaries that are epoxied to the board for mechanical and thermal isolation. Wire bonded leads are for (bulk) heating and for monitoring temperature via the patterned RTD extending into the center of the chip.

Deactivated fused-silica capillaries were sealed into the inlet/outlet ports using silicone adhesive (Duraseal 1531, Cotronics, Brooklyn, NY). Each device cavity or subsection was filled with sieved adsorbent granules using a gentle vacuum [32]. The μPCF-1 devices were loaded to capacity with either 2.3 mg of C-X or 2.0 mg of C-B. The μPCF-2 device was also loaded to capacity, the larger section with 2.0 mg of C-B and the smaller section with 1.4 mg of C-X. Adsorbent masses were determined by weighing the device with an electronic balance to ±0.1 mg before and after loading (note: since C-B has a lower density than C-X, the mass of this adsorbent contained in a given cavity volume is also lower). Devices were then mounted on custom printed circuit boards (PCB) using epoxy (Hysol 1C, Rocky Hill, CT); only the capillaries were bonded to the board to maximize thermal isolation of the device. A rectangular hole in the PCB beneath each device further improved thermal isolation. Al wire-bond wires were used for electrical connections.

3.3. Test atmospheres

Test atmospheres were generated by injecting pre-determined volumes of liquid analytes into 10-L Supel-Inert® foil-laminated gas sampling bags (Model 30240-U, Supelco), prefilled with a known volume of clean, dry N_2 from a compressed gas cylinder. Serial dilutions were made to achieve the desired range of concentrations, which were verified by a calibrated bench-scale GC with FID (Model 7890, Agilent Technologies, Palo Alto, CA). For tests performed at high humidity, small volumes of distilled water were added to the bags to achieve the desired humidity levels assuming complete vaporization.

3.4. Desorption testing

Three compounds spanning the range of p_v values of the compounds listed in Table 1 were chosen for desorption testing: benzene, toluene and n-dodecane. The effects of desorption flow rate, heating period, vapor loading, and split ratio on the desorption efficiency and bandwidth were evaluated for each VOC individually. The experimental setup for desorption testing is shown in Figs. S1a and b in the *Supporting Information* accompanying this article. Analyses were performed using the bench-scale GC-FID. μPCF-2 was mounted across two ports of a 6-port valve. A suction pump (model UMP015, KNF) was used to load the μPCF by drawing a finite air sample from the test atmosphere through the device at a low flow rate (i.e., 5 mL/min). To desorb the trapped VOCs, the valve was switched to the second position, and N_2 or He from the GC injection port was backflushed through the μPCF while it was heated at ~325 °C/s–225 °C and maintained at that temperature for varying amounts of time. This was achieved by applying 42 V across the device and using pulse width modulation with feedback from the RTD at 50 Hz to minimize overshoot and maintain a constant temperature. To be clear, for μPCF-2, the flow during sampling passed through the C-B bed first, and during desorption it was in the opposite direction.

No column was used for these single-VOC tests; the valve was plumbed directly to the FID via deactivated fused silica capillary, and both were heated to minimize any adsorption during transfer. Where separations were required, a 6-m capillary column (250-μm i.d.; 0.25-μm thick Rtx-1; Restek, Bellafonte, PA) was used. The effect of increasing the desorption flow rate while maintaining a constant flow rate to the detector was explored by splitting the flow downstream from the μPCF using a 'Y' press-tight connector. Split ratios were adjusted using the GC inlet head pressure and lengths of capillary on the vent line to create the appropriate pressure drops. Flows were measured by a miniature bubble-buret meter.

Desorption efficiency was also evaluated as a function of heating time for benzene, toluene and n-dodecane. μPCF-2 was loaded as described above with 250 ng of each analyte individually, sufficient to detect <1% residual mass with the FID. Desorption at 225 °C and 3 mL/min was continued for 20, 40, or 60 s and was followed by another desorption of similar duration after allowing the device ~2–3 min to cool to ambient temperature. The area of the first desorption was divided by the sum of the areas from both desorptions (the first desorption and any residual peak from the secondary desorption) to determine the desorption efficiency.

3.5. Breakthrough testing

Figs. S1c and d of the *Supplementary Information* show the breakthrough testing set-up, which is similar to those presented previously [22,24,26]. Test atmospheres were drawn through the μPCF and a downstream 25-μL or 250-μL sampling loop using the pump at discrete flow rates between 4 and 10 mL/min. At 30-s intervals, the six-port valve was actuated to inject the contents of the loop into the 6-m capillary column in the GC oven while the pump continued to draw sample through the μPCF. Devices were cleaned after each exposure by heating to 200 °C for 10 min under N_2 flow.

By convention, the sample volume required for the concentration downstream from the μPCF (C_x) to reach 10% of the inlet concentration (C_o), was used as the metric of the dynamic adsorption capacity of the devices, and is designated V_{b10}. This is considered the maximum sampling volume for exhaustive (quantitative) capture. All V_{b10} values were estimated to the closest 0.5 mL. Breakthrough fractions were determined by comparing the peak areas of samples obtained over the course of each test to those of samples injected directly from the test atmosphere used as the source of the challenge. The μPCF devices were thermostated for all tests by applying pulse width modulation to a 5 V bias to the on-chip heaters.

3.6. Data acquisition and management

Device heating functions were controlled, and RTD output data were collected, with a desk top computer using custom LabVIEW software written in-house. Peak parameters, including retention times, areas, heights, and full width at half height (*fwhm*) were measured using Chemstation (Rev.B.01.01, Agilent Technologies). Gaussian peak fitting and calculations of asymmetry factors were performed with OriginPro 9.1 (OriginLab, Northampton, MA). Other data processing, statistical analyses, and graphing utilized Excel (Office 2013, Microsoft).

4. Results and discussion

4.1. Desorption bandwidth

Fig. 3 shows the effect of desorption flow rate on the injection band width from μPCF-2 for benzene, toluene, and n-dodecane. Each compound was tested individually, in triplicate, by drawing a 5 mL sample of a test atmosphere containing 3–6 ppm of the compound (~50 ng) through the μPCF at 5 mL/min, reversing the direction of flow, and then heating to 225 °C in <1 s and holding for 60 s. As shown, the *fwhm* values of the desorbed peaks were inversely proportional to flow rate, with a dependence that varied inversely with p_v. The ratios of *fwhm* values at 1 and 5 mL/min were 1.8, 2.4, and 2.7 for benzene, toluene, and n-dodecane, respectively. Benzene consistently gave the sharpest peaks, but at the highest flow rate of 5 mL/min its peak was only slightly narrower than that of toluene, and only 28% narrower than that of n-dodecane.

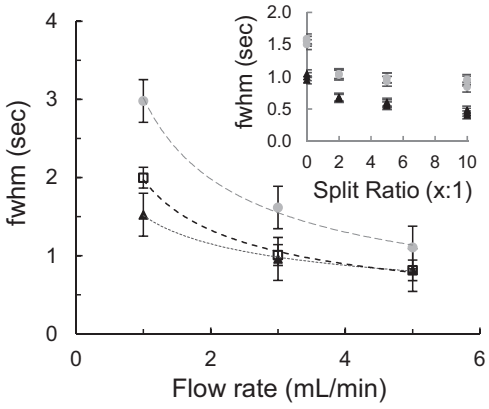

Fig. 3. Desorption bandwidth (i.e., *fwhm*) from μPCF-2 as a function of flow rate for benzene (triangles), toluene (squares), and n-dodecane (circles), tested individually without a downstream column; FID. Error bars represent 95% confidence intervals ($n = 3$). Curves represent the least-squares fits to the data. Inset shows the effect of the injection split-flow ratio (vent:analysis) on the *fwhm* values for benzene and n-dodecane; analytical path flow rate was maintained at 3.0 mL/min.

These trends are consistent with the expectation that more volatile compounds would be more rapidly and completely vaporized by the heat applied, and that compression of the desorption band would occur primarily by the increased rate at which the μPCF headspace volume was swept. The less volatile n-dodecane exhibited behavior indicative of slower or less efficient vaporization, such that the increased flow rate enhanced the rate of desorption as well as compressing the peak. These results are in qualitative agreement with those reported by Whiting and Sacks for a small packed-capillary preconcentrator device [46].

The inset in Fig. 3 shows the effect on the *fwhm* values of benzene and n-dodecane of increasing the desorption flow rate further by incorporating an injection split. By venting a portion of the downstream flow stream, sharper injections are possible without altering the flow rate passing through the GC column. For an analytical path flow rate of 3 mL/min and split ratios of 2:1, 5:1, and 10:1 (i.e., desorption flow rates of 9, 18, and 33 mL/min, respectively), the *fwhm* decreased by 33%, 42% and 55% for benzene and by 36%, 40% and 44% for n-dodecane relative to the splitless injection at 3 mL/min.

That the peak width for the more volatile benzene continued to decrease while that for the n-dodecane showed very little change beyond a split ratio of 2:1 indicates that the injection band for benzene continued to be flow rate limited while that of n-dodecane was still partially governed by the slower rate of thermal desorption from the adsorbent surface. For both compounds, the largest change in *fwhm* values occurred between no split and 2:1. Consistent with this split ratio, the observed FID peak areas for benzene and n-dodecane decreased by ~65%, whereas the peak heights decreased by only 50 and 43%, respectively. This reflects the band compression (i.e., focusing) accompanying the increase in flow rate, which at least partially offsets the loss of injected mass with respect to the peak-height sensitivity and, thus, LOD.

Increasing the initial sample volume (and mass) by 5-fold led to an increase in *fwhm* of <10% for all three vapors at 3 mL/min (splitless). At 1 mL/min the increase was greater, particularly for n-dodecane. Asymmetry factors, calculated at 10% of the peak maximum, were 1.0, 1.8 and 3.1 for benzene, toluene and n-dodecane, respectively, with splitless injection, consistent with the assertion above that thermal desorption speed and efficiency decrease with decreasing p_v value.

For n-dodecane and compounds of similar or lower volatility, on-column focusing can mitigate the effects of injection band broadening and asymmetry [47], and for compounds of somewhat higher volatility (e.g., toluene), which are not focused at the head of the column, the retention times are long enough to expect reasonable chromatographic resolution. In contrast, for benzene and similarly volatile compounds, injection band broadening has a greater influence on their resolution due to their short retention times. To evaluate the latter, in a subsequent test series, a 6-m capillary column was connected downstream from the μPCF and the chromatographic resolution (R_s) of benzene from a similarly volatile compound, trichloroethylene (TCE), was evaluated as a function of desorption flow rate and injection split ratio. Estimates of R_s ($=\Delta t_R\,[4\sigma_a]^{-1}$) were calculated from the difference in retention times, Δt_R, and the average standard deviation of the Gaussian profiles fitted to the peaks, σ_a [47].

Fig. 4a shows results for splitless injections of 50 ng of each compound at each of three flow rates. All peaks fit Gaussian profiles with $R^2 > 0.98$. Interestingly, there was little change in R_s on going from 1 to 3 mL/min; the narrowing of the peaks was accompanied by a commensurate reduction in t_R values. Since the optimal velocity for separations on this type of column corresponds to a flow rate <1 mL/min, we would have expected a decrease in R_s at the higher flow rate. Evidently, the reduction in the injection band width compensated for the loss in chromatographic efficiency over this range

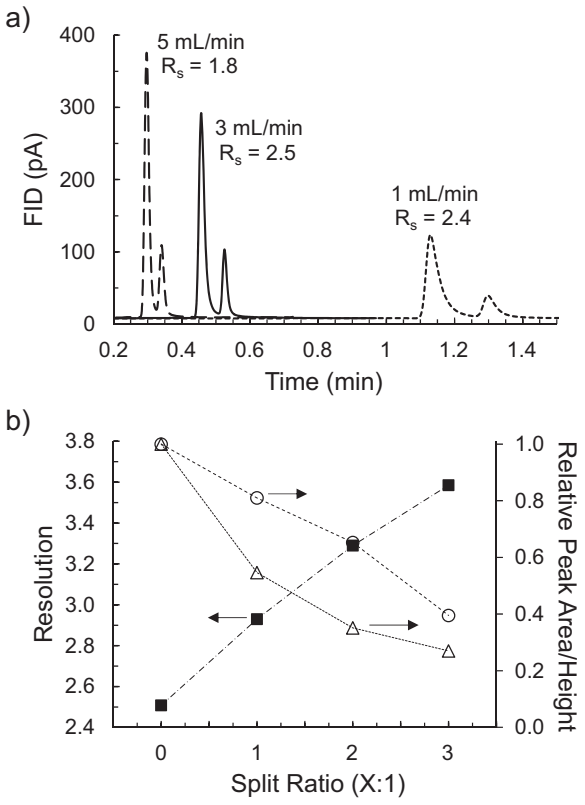

Fig. 4. (a) Superimposed chromatograms of benzene (1st peak) and trichloroethylene (2nd peak) collected at three flow rates (as indicated), with the corresponding R_s values for the pair. Samples of the binary vapor mixture (~50 ng each) were pre-loaded into μPCF-2, desorbed/injected splitless in He, and separated on a 6-m long, PDMS-coated capillary column isothermally at 30 °C; FID. (b) R_s (squares), average peak height (circles), and average peak area (triangles) for benzene and trichloroethylene plotted as a function of the injection split-flow ratio (vent:analysis), with the column (analytical path) flow rate maintained at 3.0 mL/min.

of flow rates. At 5 mL/min, however, the latter factor dominated and there was a significant decrease in R_s, consistent with the data in Fig. 3 showing relatively little reduction in the injection band width above 3 mL/min.

Fig. 4b shows the dependence of R_s and sensitivity on the injection split ratio, while maintaining a flow rate of 3 mL/min in the analytical path. The ~linear increase in R_s with the split ratio follows from Δt_R remaining constant while the widths of both peaks decreased at the same rate with increasing desorption flow rate. The tradeoff is a loss in sensitivity from venting large portions of the sample. As shown in Fig. 4b, the fractional reduction in average peak height was much less than that of average peak area because of the compression of the injection band. In any case, the relative gain in resolution (~1.4 fold) was smaller than the relative loss in sensitivity (~2.5–3 fold) over this range of split ratios, consistent with results reported in Ref. [13].

Since the responses of the CR microsensors should show the same trends in sensitivity and resolution as the FID used here [16], these results allow for a rational choice of split ratio on the basis of the specific demands of a particular analysis. That is, for a scenario involving lower concentrations of a less complex VOC mixture, a lower split ratio could be selected in favor of sensitivity, whereas for a scenario with higher concentrations of a more complex VOC mixture, a higher split ratio could be selected in favor of resolution. Of course, the sample volume is another adjustable variable that could impact such decisions (see Sections 2 and 4.3).

4.2. Desorption efficiency

Tests were then performed to determine the minimum time period required to remove all traces of analytes from the μPCF during thermal desorption. Once again, benzene, toluene, and n-dodecane were used as the test compounds to span the range of volatility expected of any samples that might be collected. Results are summarized in Table S1 of the *Supplementary Information*. Heating for 20 s was sufficient to desorb >99% of the benzene and toluene, but only 97% of the n-dodecane. For heating periods of 40 and 60 s, the desorption efficiencies of n-dodecane were 99 and >99%, respectively. Increasing the initial VOC mass loading from 250 ng to 1 μg had no effect on desorption efficiency for benzene and <1% decrease for n-dodecane. Therefore, 40 s was deemed sufficient to avoid carryover of any low volatility analytes.

4.3. Trapping capacity

Results of initial range-finding breakthrough tests conducted at 30 °C are presented in Table 2. On the basis of earlier work [23], benzene and toluene were selected as sentinel breakthrough compounds for C-X and C-B, respectively. At 5 mL/min, the average V_{b10} for benzene with the μPCF-1x device was 41 mL and the average V_{b10} value for toluene with μPCF-1b was 31 mL. Increasing the flow rate to 10 mL/min led to a decrease in V_{b10} of ≤3% in all cases, which is consistent with operation at $\tau \gg \tau_{safe}$ where the flow rate dependence of V_{b10} is expected to be small [36]. Therefore, V_{b10} values at 5 and 10 mL/min were combined in Table 2. Since the larger subsection of the μPCF-2 device holds the same mass of C-B as μPCF-1b (i.e., 2.0 mg), results from the latter are transferrable to the former. Note that previous work has shown that benzene is not retained by C-B [23], and therefore should only be trapped by the downstream C-X bed in μPCF-2. These results demonstrate that, at relatively low concentrations in the absence of co-contaminants, the individual μPCF-1 devices provide ample capacity for benzene and toluene to measure them at concentrations <50 ppb with the PEMM microsystem, assuming an LOD of ~5 ng (vide supra).

For the next set of breakthrough tests, μPCF-2 was challenged with a mixture of benzene, toluene, ethylbenzene, and xylene (i.e., BTEX), each at its respective TLV concentration except for benzene, which was at 2 × TLV to permit reliable quantification of V_{b10}. Replicate tests ($n = 3$) were performed under both dry and humid (88% relative humidity, RH) conditions in N_2. A representative set of breakthrough curves is presented in Fig. 5. Average V_{b10} values for the sentinels benzene and toluene were 33 and 90 mL, respectively (RSD < 3%). For ethylbenzene and xylene, V_{b10} was consistently >150 mL, at which point the tests were terminated. These results confirm that μPCF-2 has sufficient capacity to quantitatively retain BTEX mixtures at relevant concentrations above the 31-mL sample volume necessary to detect benzene at 0.1 × TLV.

These results are also consistent with those for individual exposures to benzene and toluene presented in Table 2; a significant decrease in V_{b10} for benzene occurred because of the smaller mass of C-X in μPCF-2, despite the lower challenge concentration (i.e., 1 ppm vs. 5 ppm), and a significant increase in V_{b10} for toluene occurred because of the downstream C-X bed in μPCF-2, despite the presence of xylene and ethylbenzene. Although it is likely that

Table 2
Values of V_{b10} for benzene and toluene tested individually at 5 ppm in dry N_2 and 30 °C with the two single-cavity μPCF devices indicated.

Device	Compound	V_{b10} [a] (mL)	RSD (%)
μPCF-1x	Benzene	41.0	1
μPCF-1b	Toluene	31.0	4

[a] Avg. of 3 replicates each at 5 and 10 mL/min.

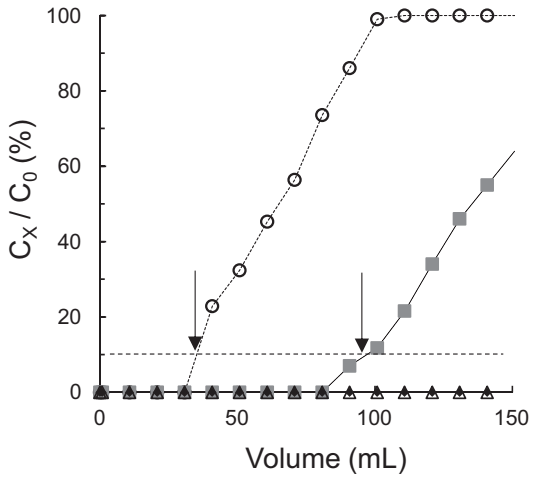

Fig. 5. Representative breakthrough curves of μPCF-2 challenged with a mixture of benzene, toluene, ethylbenzene and m-xylene (i.e., BTEX) at 1, 20, 20, and 100 ppm, respectively (i.e., TLV concentrations for all except benzene) in N_2. C_x/C_o is the breakthrough fraction. V_{b10} values for benzene (33 mL) and toluene (90 mL) are designated by the vertical arrows. V_{b10} values for ethylbenzene and m-xylene were >150 mL. *Conditions*: flow rate = 5 mL/min; temperature = 30 °C; FID.

toluene would start to displace benzene from the C-X by competitive adsorption once it breaks through the C-B bed, a larger decrease in V_{b10} for benzene would have been expected if it were an important factor. In fact, the decrease was less than expected on the basis of the reduction in adsorbent mass (vide infra). No changes in V_{b10} were observed for any of the compounds at the higher background humidity level.

The next set of breakthrough tests was designed to characterize capacity at much higher concentrations. In lieu of using a challenge test atmosphere containing a large number of compounds, mixtures of four representative compounds at higher concentrations were used. This permitted measurements at a higher frequency because chromatographic separation times were shorter. For characterizing C-X, a mixture of 2-butanone, benzene, ethyl acetate and toluene was used, and for C-B a mixture of toluene, cumene, 1,2,4-trimethylbenzene and n-dodecane was used. Within a subset, compounds were included that spanned the range of p_v values appropriate for that adsorbent material, although including toluene in the mixture for C-X was actually a more rigorous test, because the vapors intended to be captured on C-X have higher p_v values. The challenge mixtures contained 100, 150, or 200 ppm of each compound. At 200 ppm, the net (composite) mass per unit volume concentration was roughly equivalent to that of all of the target compounds in Table 1 at their respective TLV concentrations (note: since n-dodecane has no assigned TLV, a concentration of 10 ppm was assumed).

Table 3 shows the measured V_{b10} values as a function of flow rate and temperature for the subset of compounds intended to characterize the performance of the C-X bed. As expected, V_{b10} varied inversely with p_v among the test compounds under all conditions. Values of V_{b10} for the high-p_v interference 2-butanone (p_v = 13.3 kPa) were consistently the smallest observed, never exceeding 7 mL, while the values of V_{b10} for toluene consistently exceeded those of the other compounds by >2 fold. Benzene had V_{b10} values ranging from only 7.5–11 mL. For all concentrations at 30 °C there was a very slight decrease in V_{b10} with increasing flow rate as expected. V_{b10} also decreased with the 2-fold increase in C_o, but only for toluene was the decrease >12% (i.e., ~26%).

The relative insensitivity to flow rate and concentration are both predicted by the Wheeler Model [36]. The small concentration dependence reflects the increase in the dynamic adsorption capacity with increasing concentration in the sub-monolayer regime

Table 3
Values of V_{b10} for mixtures of representative VOCs drawn through μPCF-2 and μPCF-1x, as a function of concentration, temperature, and sampling flow rate.

Compound	Flow rate (mL/min)	V_{b10} (mL)						
		μPCF-2						μPCF-1x
		30 °C			100 ppm			200 ppm
		200 ppm	150 ppm	100 ppm	25 °C	35 °C	40 °C	30 °C
2-Butanone	4	4.5	5.0	5.0	5.0	3.0	2.0	7.0[a]
	6	4.5	4.5	5.0	–[b]	–	–	–
	8	4.0	4.5	4.5	–	–	–	–
	10	4.0	4.0	4.5	–	–	–	6.5
Benzene	4	8.5	8.5	9.0	9.5	4.5	3.0	11.0
	6	8.0	8.0	8.5	–	–	–	–
	8	7.5	8.0	8.5	–	–	–	–
	10	7.5	8.0	8.5	–	–	–	11.0
Ethyl acetate	4	11.0	11.5	12.0	12.5	7.0	4.5	13.5
	6	11.0	11.5	11.5	–	–	–	–
	8	10.5	11.0	11.5	–	–	–	–
	10	10.0	11.0	11.0	–	–	-	14.0
Toluene	4	27.0	32.0	37.0	46.0	27.0	17.0	45.0
	6	25.0	30.0	35.0	–	–	–	–
	8	25.0	30.0	34.0	–	–	–	–
	10	24.0	29.0	32.0	–	–	–	45.0

[a] Tested at 5 mL/min instead of 4 mL/min.
[b] Untested conditions.

where that model is applicable. The Wheeler Model also predicts the breakthrough volume to increase in proportion to the bed mass. The ratios of V_{b10} for the μPCF-1x and μPCF-2 devices at 200 ppm were, on average, slightly lower than the ratio of adsorbent masses in these two devices (mass ratio = 1.6) for the three more volatile compounds, mostly likely because of competitive adsorption. Since toluene was partially retained on the C-B bed of μPCF-2 it cannot be included in these comparisons.

Temperature had a large impact on V_{b10} for all compounds; an increase from 25 to 40 °C, which corresponds to only a 5% increase on the Kelvin scale (i.e., 313/298) resulted in reductions of 2.5–3.2 fold in V_{b10} among the C-X test compounds. Since diffusion coefficients *increase* with temperature, the loss in capacity must be due to a decrease in the dynamic adsorption capacity, which should vary as $e^{-\alpha T}$, where T is temperature in Kelvin and α is proportional to the enthalpy of adsorption [48]. These results serve to highlight the importance of maintaining the μPCF-2 device at a low temperature and, in particular, to allow it sufficient time to cool down after each injection prior to starting to collect the subsequent sample with the PEMM prototype.

We note that V_{b10} for benzene with μPCF-2 at 30 °C did not reach the benchmark value of 10 mL for any of these high-concentration challenge mixtures, but that it reached 11 mL with μPCF-1x due to the increase in the C-X bed mass. Similarly, the ethyl acetate V_{b10} values, which barely exceeded the benchmark value with uPCF-2, increased significantly with μPCF-1x. Although the V_{b10} estimates obtained by testing with these high VOC concentrations are conservative, affording some margin of safety for cases in which additional compounds of similar or lower volatility might be present, these results led us to conclude that the bed mass of C-X in the next-generation dual-cavity μPCF devices to be installed in the PEMM prototype must be increased to 2.3 mg.

Table 4 presents the measured V_{b10} values as a function of flow rate and temperature for the compounds intended to characterize the performance of the C-B. As above, μPCF-1b was used as a surrogate device that held the same mass of C-B as the large subsection of μPCF-2. For these tests only one mixture was used, with each component at 200 ppm. Once again, V_{b10} consistently varied inversely with p_v among the test compounds. Since results at 5 and 10 mL/min were not significantly different, they were combined in Table 4. At 30 °C, V_{b10} ranged from 12 mL for the sentinel toluene to >150 mL for the least volatile n-dodecane. As was found for the tests with C-X, V_{b10} decreased with increasing temperature, but at a much lower rate, decreasing by <20% in all cases for an increase from 30 to 40 °C. The V_{b10} value for n-dodecane remained >150 mL under all conditions.

Interestingly, V_{b10} for toluene with C-B decreased by about 2.5-fold relative to the value presented in Table 2, which was obtained at a much lower concentration in the absence of co-contaminants. However, even at the high concentrations tested here in the presence of high concentrations of co-contaminants, the V_{b10} value exceeds the 10 mL benchmark value. Of course, as shown in Table 3 and Fig. 5, toluene would be trapped effectively on the downstream C-X bed at larger sample volumes, but this situation should ideally be avoided, because it might lead to injection band broadening due to the stronger adsorption of toluene on C-X. Thus, we conclude that 2.0 mg of C-B is sufficient for trapping the less volatile fraction of anticipated VOC mixtures, and the next-generation μPCF to be used in the PEMM prototype should be designed to hold this mass of C-B.

4.4. Sampling and analysis of the 17-VOC mixture

The performance of μPCF-2 was then evaluated with a test atmosphere containing a mixture of the 17 compounds in Table 1, each at 10 ppm to facilitate rapid separation and detection of low breakthrough fractions with the downstream capillary column and FID. The sampling flow rate was 5 mL/min and the test

Table 4
Values of V_{b10} for a mixture of representative VOCs (200 ppm each) with μPCF-1b as a function of temperature.

Compound	V_{b10} (mL)[a]		
	30 °C	35 °C	40 °C
Toluene	12.0	11.5	9.5
Cumene	23.0	22.0	20.0
1,2,4-Trimethylbenzene	82.5	80.5	78.0
n-Dodecane	>150	>150	>150

[a] Avg. of 3 replicates each at 5 and 10 mL/min (RSD < 3% in all cases).

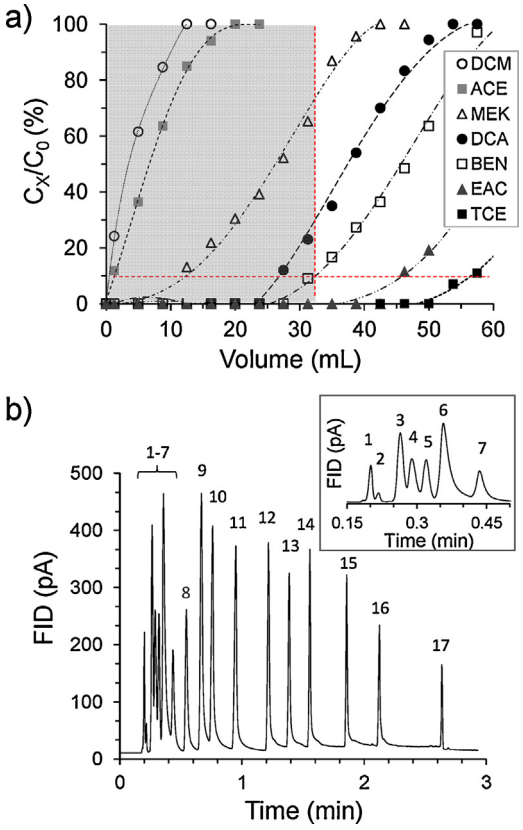

Fig. 6. (a) Breakthrough curves of μPCF-2 challenged with the 17-VOC mixture (see Table 1 for acronym definitions) at 30 °C and 5 mL/min with C_o = 10 ppm for each compound; only the first seven compounds to break through were monitored. Shaded region corresponds to $V \leq V_{b10}$ for benzene. (b) Chromatogram of a 20-mL sample of the same 17-VOC test atmosphere injected from μPCF-2 and separated on a 6-m capillary column; inset shows enlargement of the first seven compounds to elute (see Table 1 for peak # assignments). *Conditions*: 3 mL/min; 2:1 split injection; column held at 28 °C for 0.5 min, then 10 °C/min to 33 °C, then 50 °C/min to 125 °C.

was concluded when the total sample volume reached 60 mL. The breakthrough curves in Fig. 6a demonstrate the partial selectivity against high-p_v compounds: the V_{b10} values of dichloromethane, acetone, and 2-butanone were all smaller than that of benzene, and the former two compounds reached 100% breakthrough prior to V_{b10} for benzene. Although a fraction of the sampled mass of each of these compounds was retained, it was much lower than that of the sentinel benzene and other targets. Surprisingly, the V_{b10} of 1,2-dichloroethane was also slightly smaller than that of the more volatile benzene, which can be ascribed to the dipolarity of this compound and consequent lower affinity for the non-polar C-X surface. Despite the presence of several compounds competing for adsorption sites on the C-X, the V_{b10} of benzene was still 31 mL.

Fig. 6b shows the chromatogram obtained by sampling at 5 mL/min for 4 min through the μPCF-2, followed by heating, back flushing, and injecting the sample with a 2:1 split and an analytical path flow rate of 3 mL/min of He. A 20-mL sample volume was used for convenience to illustrate the selective preconcentration and, at the same time, generate reasonably large peaks for all compounds. As shown, all 17 compounds were separated in <3 min. Acetone and dichloromethane eluted first and gave much smaller peaks due to selective preconcentration. The 2-butanone eluted next and gave a large peak due to its being retained to a greater extent than the other two interferences. The remaining 14 compounds were captured quantitatively from the 20 mL sample (see Fig. 6a; total mass of ~12 μg) and the injected mass of each ranged from 630 to 1380 ng prior to the split. Notably, both 1,2-dichloroethane and ethyl acetate eluted before benzene due to their higher polarity, and gave somewhat smaller peaks, presumably due to their having smaller response factors in the FID [47].

Among the 14 targets the chromatographic resolution was quite good, with values of R_s > 1.0 in all cases. Prior work demonstrated about a 10% reduction in resolution of early eluting peaks for the microcolumns to be used in the PEMM prototype relative to a commercial capillary like that used here, indicating that the separation of similar mixtures should be comparable. The inset in Fig. 6b shows that the first six compounds were separated in <24 s. Some tailing was evident in all of the peaks, but asymmetry factors were <1.6 in all cases due, in part, to the sharp split injection. The small *fwhm* values of peaks 13–17 (i.e., 0.8–1.3 s) reflect the influence of on-column focusing at the outset of the separation. The somewhat larger *fwhm* values of peaks 7–12 (i.e., 1.2–1.7 s) reflect the fact that these compounds are too volatile to be focused, and they have wider effective injection bands and spend more time on the column than the more volatile compounds (i.e., peaks 4–6) for which *fwhm* ranged from 0.8 to 1.1 s. Regardless, none of the peaks is excessively broad and all are well separated. Moreover, there is additional space available in the mid-range of the chromatogram to accommodate other compounds that might be encountered in practice in this volatility range.

4.5. Preconcentration factors (PF)

Assuming no breakthrough, the PF is the ratio of the volume of the air sample collected to the volume in which that same mass is contained at the point of detection [41,42]. The latter can be taken as the volume of the peak generated directly from the injection or after chromatographic separation. The latter volume will differ from the former due to on-column focusing or broadening of the injection band, but using it to determine an "effective PF", while less rigorous, is more practical, since all analyses will include a separation step prior to detection. Note that the practice of calculating "preconcentration factors" from the ratio of peak areas generated with and without a μPCF included in the system [31,34] is not recommended, because it does not afford any useful information about the critical performance parameters of a μPCF.

For the most volatile target, benzene, an injection *fwhm* value of 0.90 s was obtained at 3 mL/min (no split), which corresponds to a preconcentrated volume of 0.048 mL. Assuming a 31-mL sample volume, then we obtain a PF value of ~620 for benzene. For our least volatile target, n-dodecane, the injection *fwhm* value was ~1.7 s at 3 mL/min (no split), which corresponds to a peak volume of 0.085 mL. For a sample volume of 31 mL, this yields a PF value of only 370. Note, however, that V_{b10} for n-dodecane was >150 mL under all conditions tested. Increasing the assumed sample volume to 150 mL leads to a PF of 1590, even after allowing for a 10% increase in the *fwhm* value of the peak at the higher injection mass.

If an injection split were used, then there would be a commensurate reduction in PF due to the loss of sample mass, which would greatly exceed the decrease in *fwhm* afforded by the split (see Fig. 4b). For example, from Fig. 6b, the *fwhm* values of benzene and n-dodecane after separation on a 6-m column at 3 mL/min with a 2:1 injection split were 1.5 and 1.9 s, respectively. The effective PF values using the corresponding peak volumes of 0.076 mL and 0.097 mL together with the 20 mL sample volume, were only 88 and 68 for benzene and n-dodecane, respectively, reflecting the small sample volume and the loss of ~67% of the sample from the split injection.

5. Conclusions

The design and operating features of the μPCF developed here meet or exceed the requirements of this component of the

(wearable) μGC into which it will be integrated for the specific application of quantitatively analyzing exposures to mixtures of VOCs encountered in workplace environments. Thus, a dual-cavity μPCF containing 2.0 and 2.3 mg of C-B and C-X, respectively, operated at a flow rate of 5–10 mL/min yields V_{b10} values ranging from ~10 mL to >40 mL for mixtures of ~10–20 compounds in the designated volatility range, with preconcentration factors of ~200–1600 and sampling times of ≤5 min.

The approach taken here has entailed careful consideration of device-level and system-level factors, fluidic and thermal factors, and numerous application-specific variables in resolving the trade-offs in selectivity, capacity, desorption efficiency, and desorption bandwidth, which are the critical performance metrics. This study complements others from our group on this topic [23–26,32,35,36], by further elucidating and addressing the details of μPCF design and implementation in high-performance micro-analytical systems for VOC mixture determinations.

Delimiting the range of target compounds on the basis of volatility (i.e., p_v values from 0.03 to 13 kPa) was rationalized on practical and fundamental grounds, and is a common, if not requisite, feature of fieldable μGC instrumentation; inherent constraints on the complexity of mixtures that can be analyzed by such instrumentation demand such concessions [12–16,20]. Delimiting the concentration range for any specific VOC in terms of its ACGIH TLV value (i.e., 0.1–2 × TLV) was also rationalized on practical grounds, though proved difficult to implement because it translated into a concentration range $>10^4$ when all target compounds were considered collectively. This will likely demand the designation of two operating modes (i.e., "high" and "low" concentration) for the μGC, which will differ in sample volume.

Selectivity against high-volatility interferences was achieved/demonstrated while retaining the capability for exhaustive capture of target compounds, in mixtures, at relevant concentrations. The breakthrough volumes and associated quantities of target compounds captured (and subsequently thermally desorbed) were sufficiently large to ensure detection at <0.1 TLV by the microsensor array to be used as the μGC detectors. Conditions established for desorption and injection into a downstream separation column ensured >99% desorption efficiency and injection bandwidths narrow enough to permit high chromatographic resolution of mixture components. The latter could be enhanced by use of split injection in cases where the accompanying loss in sensitivity could be tolerated. Given that the PEMM prototype is being designed to operate in a variety of occupational settings and to monitor a variety of possible VOC mixtures, the capability for adjusting the split ratio is to be incorporated via a metering valve downstream from the μPCF.

On-going work is directed at characterizing the next-generation dual-cavity μPCF devices that have been fabricated on the basis of the results from this study. A new heater design provides higher heating rates and consequently sharper injection bands than in the μPCF-2 devices used here, with lower power dissipation, despite the larger C-X bed mass. Implementation of an upstream pre-trap for removing low-volatility (p_v < 0.03 kPa) interferences is also underway. This will be followed by assembly and characterization of the first PEMM μGC prototype.

Acknowledgments

The authors gratefully acknowledge Ms. Katharine Beach for device fabrication, Mr. Robert Gordenker and Dr. Jung Hwan Seo for input on device design features, and Mr. Nicolas Nuñovero for electronic hardware and software during testing. This work was supported by Grant R01-OH010297 from the National Institute for Occupational Safety and Health of the Centers for Disease Control and Prevention (NIOSH-CDCP). JB-G was supported by Training Grant T42-OH008455 from NIOSH-CDCP. The sponsoring organization had no role in the design or conduct of this research. Devices were fabricated in the Lurie Nanofabrication Facility, a member of the National Nanotechnology Infrastructure Network, which is supported by the National Science Foundation.

Appendix A. Supplementary data

Supplementary data associated with this article can be found, in the online version, at http://dx.doi.org/10.1016/j.chroma.2015.10.045.

References

[1] J.S. Ignatio, W.H. Bullock (Eds.), A Strategy for Assessing and Managing Occupational Exposures, 3rd ed., AIHA Press, Fairfield, VA, 2006.
[2] J.L. Perkins, Modern Industrial Hygiene – Vol. 1. Recognition and Evaluation of Chemical Agents, 2nd ed., ACGIH, Cincinnati, OH, 2008.
[3] National Institute for Occupational Safety and Health, NIOSH Manual of Analytical Methods, http://www.cdc.gov/niosh/docs/2003-154/ (accessed May 2015).
[4] Occupational Safety and Health Administration, Sampling and Analytical Methods, https://www.osha.gov/dts/sltc/methods/ (accessed May 2015).
[5] D.H. Anna, The Occupational Environment: Its Evaluation, Control, and Management, vol. 1, 3rd ed., AIHA, Fairfax, VA, 2011.
[6] Griffin 460, FLIR Systems, Available at www.flir.com/threatDetection/display/?id=63281 (accessed July 2015).
[7] Gasmet DX4040, Gasmet Technologies, Available at www.gasmet.com/products/portable-gas-analyzers (accessed May 2015).
[8] HAPSITE ER, Inficon, Available at http://products.inficon.com/en-us/nav-products (accessed May 2015).
[9] Tridion™-9 GC–MS, Torion, Available at http://www.torion.com/products (accessed May 2015).
[10] S.C. Terry, H. Jermann, J. Angel, A gas chromatograph air analyzer fabricated on a silicon wafer, IEEE Trans. Electron Dev. 26 (1979) 1880–1887.
[11] E.S. Kolesar, R.R. Reston, Review and summary of a silicon micromachined gas chromatography system, Proc. IEEE Trans. Comp. Packag. Manuf. Technol. B 21 (1998) 324–328.
[12] R.P. Manginell, J.M. Bauer, M.W. Moorman, L.J. Sanchez, J.M. Anderson, J.J. Whiting, D.A. Porter, D. Copic, K.E. Achyuthan, A monolithically-integrated μGC chemical sensor system, Sensors 11 (2011) 6517–6532.
[13] C.-J. Lu, W.H. Steinecker, W.-C. Tian, M.C. Oborny, J.M. Nichols, M. Agah, J.A. Potkay, H.K.L. Chan, J. Driscoll, R.D. Sacks, K.D. Wise, S.W. Pang, E.T. Zellers, First-generation hybrid MEMS gas chromatograph, Lab Chip 5 (2005) 1123–1131.
[14] P.R. Lewis, R.P. Manginell, D.R. Adkins, R.J. Kottenstette, D.R. Wheeler, S.S. Sokolowski, D.E. Trudell, J.E. Bymes, M. Okandan, J.M. Bauer, R.G. Manley, G.C. Frye-Mason, Recent advancements in the gas-phase μChem Lab, IEEE Sens. J. 6 (2006) 784–795.
[15] S. Zampolli, I. Elmi, F. Mancarella, P. Betti, E. Dalcanale, G.C. Cardinali, M. Severi, Real-time monitoring of sub-ppb concentrations of aromatic volatiles with a MEMS-enabled miniaturized gas-chromatograph, Sens. Actuators B: Chem. 141 (2009) 322–328.
[16] S.K. Kim, D.R. Burris, H. Chang, J. Bryant-Genevier, E.T. Zellers, Microfabricated gas chromatograph for on-site determinations of trichloroethylene in indoor air arising from vapor intrusion, Part 1: Field evaluation, Environ. Sci. Technol. 46 (2012) 6065–6072.
[17] J. Liu, J.H. Seo, Y.B. Li, D. Chen, K. Kurabayashi, X.D. Fan, Smart multi-channel two-dimensional micro-gas chromatography for rapid workplace hazardous volatile organic compounds measurement, Lab Chip 13 (5) (2013) 818–825.
[18] B.X. Chen, T.Y. Hung, R.S. Jian, C.-J. Lu, A multidimensional micro gas chromatograph employing a parallel separation multi-column chip and stop-flow μGC × μGCs configuration, Lab Chip 13 (7) (2013) 1333–1341.
[19] Y.T. Qin, Y.B. Gianchandani, iGC1: an integrated fluidic system for gas chromatography including knudsen pump, preconcentrator, column, and detector microfabricated by a three-mask process, J. Microelectromech. Syst. 23 (4) (2014) 980–990.
[20] W.R. Collin, G. Serrano, L.K. Wright, H. Chang, N. Nuñovero, E.T. Zellers, Microfabricated gas chromatograph for rapid, trace-level determinations of gas phase explosive marker compounds, Anal. Chem. 86 (2014) 655–663.
[21] W. Collin, A. Bondy, D. Paul, K. Kurabayashi, E.T. Zellers, μGC × μGC: comprehensive two-dimensional gas chromatographic separations with microfabricated components, Anal. Chem. 87 (3) (2015) 1630–1637.
[22] A. Garga, M. Akbar, E. Vejerano, S. Narayanan, L. Nazhandali, L.C. Marr, M. Agah, G.C. Zebra, A mini gas chromatography system for trace-level determination of hazardous pollutants, Sens. Actuators B: Chem. 212 (2015) 145–154.
[23] C.-J. Lu, E.T. Zellers, A dual-adsorbent preconcentrator for a portable indoor-VOC microsensor system, Anal. Chem. 73 (2001) 3449–3457.
[24] C.-J. Lu, E.T. Zellers, Multi-adsorbent preconcentration/focusing module for portable-GC/microsensor-array analysis of complex vapor mixtures, Analyst 127 (2002) 1061–1068.

[25] W.-C. Tian, S. Pang, C.-J. Lu, E.T. Zellers, Microfabricated preconcentrator-focuser for a microscale gas chromatograph, J. Microelectromech. Syst. 12 (2003) 264–272.
[26] W.C. Tian, H.K.L. Chan, C.-J. Lu, S.W. Pang, E.T. Zellers, Microfabricated multi-stage preconcentrator-focuser for a micro gas chromatograph, J. Microelectromech. Syst. 14 (2005) 498–507.
[27] M. Kim, S. Mitra, A microfabricated microconcentrator for sensors and gas chromatography, J. Chromatogr. A 996 (2003) 1–11.
[28] R.P. Manginell, D. Adkins, M.W. Moorman, R. Hadizadeh, D. Copic, D.A. Porter, J.M. Anderson, V.M. Hietala, J.R. Bryan, D.R. Wheeler, K.B. Pfeifer, A. Rumpf, Mass sensitive microfabricated chemical preconcentrator, J. Microelectromech. Syst. 17 (6) (2008) 1396–1407.
[29] C.M. Hussain, C. Saridara, S. Mitra, Carbon nanotubes as sorbents for the gas phase preconcentration of semivolatile organics in a microtrap, Analyst 133 (2008) 1076–1082.
[30] I. Gracia, P. Ivanov, F. Blanco, N. Sabate, X. Vilanova, X. Correig, L. Fonseca, E. Figueras, J. Santander, C. Cane, Sub-ppm gas sensor detection via spiral μ-preconcentrator, Sens. Actuators B: Chem. 132 (2008) 149–154.
[31] B. Alfeeli, M. Agah, MEMS-based selective preconcentration of trace level breath analytes, IEEE Sens. J. 9 (2009) 1068–1075.
[32] T. Sukaew, H. Chang, G. Serrano, E.T. Zellers, Multi-stage preconcentrator/focuser module designed to enable trace level determinations of trichloroethylene in indoor air with a microfabricated gas chromatograph, Analyst 136 (2011) 1664–1674.
[33] W.-C. Tian, T.H. Wu, C.-J. Lu, W.R. Chen, H.J. Sheen, A novel micropreconcentrator employing a laminar flow patterned heater for micro gas chromatography, J. Microelectromech. Syst. 22 (6) (2012) 1–8.
[34] M.Y. Wong, W.R. Cheng, M.H. Liu, W.C. Tian, C.J. Lu, A preconcentrator chip employing μSPME array coated with in-situ-synthesized carbon adsorbent film for VOCs analysis, Talanta 101 (2012) 307–313.
[35] G. Serrano, T. Sukaew, E.T. Zellers, Hybrid preconcentration/focuser module for determinations of explosive marker compounds with a micro-scale gas chromatograph, J. Chromatogr. A 1279 (2013) 76–85.
[36] T. Sukaew, E.T. Zellers, Evaluating the dynamic retention capacities of microfabricated vapor preconcentrators as a function of flow rate, Sens. Actuators B: Chem. 183 (2013) 163–171.
[37] J.H. Seo, S.K. Kim, E.T. Zellers, K. Kurabayashi, Microfabricated passive vapor preconcentrator/injector designed for micro gas chromatography, Lab Chip 12 (4) (2012) 717–724.
[38] H. Lahlou, X. Vilanova, X. Correig, Gas phase micro-preconcentrators for benzene monitoring: a review, Sens. Actuators B: Chem. 176 (2014) 198–210.
[39] H. Lord, J. Pawliszyn, Evolution of solid-phase microextraction technology, J. Chromatogr. A 885 (1–2) (2000) 153–193.
[40] M. Chai, J. Pawlinszyn, Analysis of environmental air samples by solid-phase microextraction and gas-chromatography ion-trap mass-spectrometry, Environ. Sci. Technol. 29 (3) (1995) 693–701.
[41] International Union of Pure and Applied Chemistry, Compendium of Chemical Terminology Gold Book, 2.3.3, 2004, pp. 1174–1175, Available at goldbook.iupac.org/P04804 (accessed May 2015).
[42] J. Namieśnik, Preconcentration of gaseous organic pollutants in the atmosphere, Talanta 35 (7) (1988) 567–587.
[43] ACGIH, Threshold Limit Values for Chemical Substances and Physical Agents & Biological Exposure Indices for 2015, ACGIH, Cincinnati, OH, 2015.
[44] Q. Zhong, W. Steinecker, E.T. Zellers, Characterization of a high-performance portable GC with a chemiresistor array detector, Analyst 134 (2009) 283–293.
[45] S.K. Kim, H. Chang, E.T. Zellers, Microfabricated gas chromatograph for the selective determination of trichloroethylene vapor at sub-parts-per-billion concentrations in complex mixtures, Anal. Chem. 83 (2011) 7198–7206.
[46] J. Whiting, R. Sacks, Evaluation of split/splitless operation and rapid heating of a multi-bed sorption trap used for gas chromatography analysis of large-volume air samples, J. Sep. Sci. 29 (2006) 218–227.
[47] R.L. Grob, E.F. Barry, Modern practice of gas chromatography, 4th ed., Wiley Interscience, Hoboken, NJ, 2004, pp. 114–115.
[48] C. Zhou, Y. Jin, H. Xu, S. Feng, G. Zhou, J. Liang, J. Xu, Use of Wheeler-Jonas equation to explain xenon dynamic adsorption breakthrough curve on granular activated carbon, J. Radioanal. Nucl. Chem. 288 (2011) 251–256.